Reducing the number of size classes in a cumulative rates model used for process control of a grinding mill circuit

J.D. le Roux[a,*], I.K. Craig[a]

[a]*Department of Electrical, Electronic, and Computer Engineering, University of Pretoria, Pretoria, South Africa.*

Abstract

The number of size classes in a cumulative rates model of a grinding mill circuit is reduced to determine the minimum number required to provide a reasonably accurate model of the circuit for process control. Each reduced size class set is used to create a non-linear cumulative rates model which is linearised to design a linear model predictive controller. The accuracy of a model is determined by the ability of the corresponding model predictive controller to control important process variables in the grinding mill circuit as represented by the full non-linear cumulative rates model.

Results show that a model with 25 size classes that provides valuable information for plant design and scale-up, can be reduced to a model containing only a small number of size class sets and still be suitable for process control. Although as few as 3 size classes can be used to obtain a fairly accurate model for process control, the distribution of these 3 size classes influences the accuracy of the model. For a model to be useful for process control, the model should at least provide the directions in which the process variables change.

Keywords: comminution, grinding, modelling, model reduction

1. Introduction

When modelling a grinding mill circuit with a population balance model, the question arises how many and which size classes should be used to characterize the material in the circuit. The studies of Amestica et al. (1996) and Apelt et al. (2002) use 27 size classes in their models, the model of le Roux et al. (2013) uses only 3 size classes and the model of Bascur and Herbst (1985) uses only 2 size classes to characterize ore. The latter two models were developed for process control purposes and the model in le Roux et al. (2013) has been used in a robust nonlinear model predictive controller for a grinding mill circuit (Coetzee et al., 2010). The advantage of a model with fewer size classes is that it is simpler to incorporate in a model-based controller scheme. However, a model-based controller is dependent on an accurate and reliable process model. Therefore, it is of interest to determine the minimum number of size classes that yields a good model for process control purposes.

It can be argued that a model should have a minimum of four or five size classes. The size classes should account for the usually bimodal size distributions of run-of-mine ore feed, mill discharge and hold-up. The size classes should therefore reflect the following:

- Slimes from zero to a few microns that have transport behaviour that follows that of water. The model of Apelt et al. (2002) assumes that the specific discharge rate function is constant up to about 1 mm.

- Fines from a few microns to around 13-25 mm that should obey normal breakage behaviour and would be the typical feed for a conventional ball mill.

- Critical size material from 13-25 mm to 50-100 mm that exhibits abnormal breakage behaviour. This material does not self-break, is difficult to grind and is inefficiently broken by coarse rock and steel grinding media. This is particularly true for fully-autogenous (FAG) and semi-autogenous (SAG) mills.

- Rocks coarser than about 100 mm that self-breaks to form pebble grinding media, but leads to critical size problems.

This article investigates how many size classes are necessary to accurately simulate a grinding mill circuit with a cumulative rates model for process control purposes. The study uses the sampling campaign data of an optimisation study of an industrial circuit treating Merensky ore (Hinde, 2009). A base set of 25 size classes is reduced to smaller sets and each reduced set is used to model the circuit. Since the cumulative rates model is non-linear, each model is linearized before it is used to design a linear model-based controller. The controllers are implemented on a grinding mill circuit simulated by the

_____

*Corresponding author. Address: Department of Electrical, Electronic and Computer Engineering, University of Pretoria, Pretoria, South Africa.
Tel.: +27 12 420 2201; Fax: +27 12 362 5000.
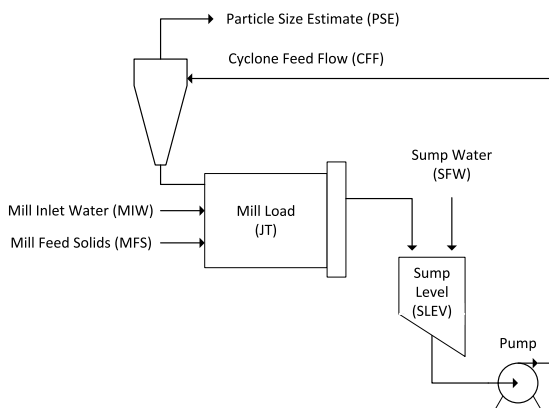*Email address:* derik.leroux@up.ac.za (J.D. le Roux)

Figure 1: A single-stage closed grinding mill circuit where the manipulated variables are MIW, MFS, SFW, and CFF, and the controlled variables are PSE, $SLEV$ and JT.

Table 1: Description of circuit variables.

Variable	Description
Manipulated Variables	
CFF	flow-rate of slurry to the cyclone [m^3/h]
MFS	feed-rate of ore to the mill [t/h]
MIW	flow-rate of water to the mill [m^3/h]
SFW	flow-rate of water to the sump [m^3/h]
Controlled Variables	
JT	fractional volumetric filling of mill [%]
PSE	product particle size estimate [fraction $\leq$ 75 μm]
$SLEV$	slurry level in sump [m]

non-linear model with 25 size classes. The controller performance is used as a measure of the accuracy with which a size class set models the circuit. Because the controllers are model-based, the performance also indicates the least number of size classes that should be included in a model for process control.

2. Grinding Mill Circuit Description

According to the survey by (Wei and Craig, 2009) ball mills are most common in industrial plants, followed closely by FAG and SAG mills. A ball mill is usually fed with crushed ore, whereas SAG and FAG mills are fed with ROM ore. In FAG mills the grinding media consists only of ore, whereas ball and SAG mills are fed with steel balls to assist with ore breakage (Stanley, 1987). A ROM ore SAG mill with a high ball load and an end-discharge screen in a single-stage closed circuit configuration, as shown in Fig. 1, is considered for this study.

The three main elements in Fig. 1 are the mill, the sump and the hydrocyclone. The mill receives four streams: mined ore (MFS), water (MIW), steel balls and underflow from the hydrocyclone. The ground ore in the mill mixes with the water to create a slurry. The fraction of the mill volume filled with charge is represented by JT. The slurry is then discharged to the sump. The slurry from the mill can be discharged either by overflow or through an end-discharge screen. In the case of the screen, the particle size of the discharged slurry from the mill is limited by the aperture size of the screen. The slurry level in the sump is represented by $SLEV$. The slurry in the sump is diluted with water (SFW) before it is pumped to the cyclone for classification. The outflow of the pump is the classifier feed flow CFF. The hydrocyclone is responsible for the separation of the in-specification and out-of-specification ore discharged from the sump. The lighter, smaller and in-specification particles of the slurry pass to the overflow

of the hydrocyclone, while the heavier, larger and out-of-specification particles pass to the underflow. The underflow is passed to the mill for further grinding. The overflow contains the final product, measured in terms of the fraction of particles smaller than the specification size (PSE), that is passed to a downstream process (Coetzee et al., 2010; Stanley, 1987).

A description of the variables in Fig. 1 and their respective units can be found in Table 1. These variables are commonly controlled and manipulated in grinding mill circuits (Wei and Craig, 2009).

3. The Cumulative Rates Model

The cumulative rates model in Hinde and Kalala (2009) is a simple population balance model based on the assumption that only one function is necessary to describe grinding kinetics inside the mill, as illustrated in Bascur and Herbst (1985). This function is the cumulative breakage rate function, which is defined as the rate per unit mass that a given species coarser than a given size breaks to below that size (Austin et al., 1993). This assumption gives an advantage over the population balance model of Whiten (1974) and Apelt et al. (2002) which require two functions, the breakage rate and the appearance function, to describe the grinding kinetics. The parameters of the breakage function in the cumulative breakage rate model can be back calculated from plant measurements (Hinde and Kalala, 2009).

The cumulative rates model has been successfully used to simulate a SAG grinding mill circuit in Amestica et al. (1993, 1996). A dynamic simulator based on the cumulative rates model was coupled to an on-line parameter estimator and validated in simulation with industrial plant data in Salazar et al. (2009). The cumulative rates model was also used by Hinde and Pearson (2001) and Hinde (2009) to improve the operating performance of industrial grinding mill circuits. A discussion of the application of this model to SAG mills can be found in Hinde and Kalala (2009).

A drawback in the cumulative breakage rate model is the assumption that the cumulative rates of breakage of

ore above a given size x_i is unaffected by the grinding environment and the structure of the size distribution above x_i. This drawback also holds for the parameters of the breakage rate and appearance function of the models of Whiten (1974) and Apelt et al. (2002). If grinding conditions depart significantly from those used to derive the cumulative breakage rate parameters, it is possible to get negative flow rates in some of the size classes - especially the smaller size classes. This implies that the parameters need to be adjusted according to the changes in the grinding conditions. Including the effect of grinding environment changes on the cumulative breakage rate function is a possible improvement of the model, but does not form part of this study. It can be assumed that for a SAG mill the values for the cumulative breakage rate function remain fairly constant as long as the ball filling and internal charge level remain fairly constant (Amestica et al., 1993).

3.1. Cumulative Rates Model Description

The circuit shown in Fig. 1 with variables described in Table 1, is considered in this study. The cumulative rates model of Hinde and Kalala (2009), as it defines the mill, the sump and the hydrocyclone in Fig. 1, is described here. The nomenclature of the model can be seen in Table 2.

3.1.1. Mill model

For the cumulative rates model particle sizes are reported as the cumulative percentage of ore smaller than size x_i (mm). The first and largest size x_1 is selected to be larger than the largest particles likely to be encountered in the feed stream. The sink size class n represents all particles with sizes between zero and x_n (Hinde and Kalala, 2009).

The specific cumulative breakage rate function K_i is the fractional rate at which particles above a given size x_i in the mill break to below that size per unit time. The energy-normalised cumulative breakage rate function is given by $K_i^E = (M/P) K_i$ and is generally insensitive to scale-up (Amestica et al., 1993). M (t) is the ore hold-up in the mill and P (kW) is the net mill power. The unit for K_i^E is $[\text{kWh/t}]^{-1}$.

The mill model considers a continuously fed mill and treats it as a single fully mixed reactor. The population balance equation with respect to time for size class 1 is:

$$\frac{dw_1}{dt} = f_1 - g_1 w_1 - w_1 \frac{P}{M} K_2^E \qquad (1)$$

where w_i (t) is the absolute mass retained in size class i, f_i (t/h) is the absolute mass flow-rate for the mill feed for size class i and g_i (h^{-1}) is the specific discharge rate for size class i. Since there are no particles larger than x_1, K_1^E is undefined and K_2^E is used in eq. (1) to describe the breakage of ore in size class 1 to smaller sizes.

Table 2: Nomenclature for cumulative rates model.

Parameter	Description
α_{speed}	Fraction of critical mill speed
D	Inside diameter of mill [m]
ε_c	Effective static porosity of the charge
f_0	Absolute mass flow of water in the feed stream [t/h]
f_i	Absolute mass flow of ore in size class i in the feed stream [t/h]
g_0	Specific discharge rate for water [h^{-1}]
g_i	Specific discharge rate for size class i [h^{-1}]
g_{max}	Specific discharge rate for water and ore sizes up to x_m [h^{-1}]
J_T	Static fractional volumetric filling for total charge
J_B	Static fractional volumetric filling of mill for balls
K_i^E	Energy-normalised cumulative breakage rate [kWh/t]$^{-1}$
L	Inside length of mill [m]
M	Ore hold-up [t]
P_{mill}	Net mill power [kW]
ρ_B	Density of balls [t/m^3]
ρ_S	Density of ore [t/m^3]
v_{mill}	Internal mill volume [m^3]
w_0	Absolute mass of water in the mill [t]
w_b	Mass of balls inside the mill [t]
w_c	Weight of ore as fraction of total mass of ore and water in the mill
w_i	Absolute mass of ore retained in size class i in the mill [t]
x_g	Effective mesh size of the grate above which discharge is zero [mm]
x_i	Size of size class i [mm]
ϕ	Volume percentage solids in the cyclone feed pulp
r_i	Flow-rate of material in size class i into the sump [m^3/h]
s_0	Flow-rate of water out of the sump [m^3/h]
s_i	Flow-rate of material in size class i out of the sump [m^3/h]
v_{pulp}	Total volume of pulp in the sump [m^3]

The rate of change of the hold-up of material coarser than x_i is given by:

$$\frac{dW_i}{dt} = F_i - G_i - W_i \frac{P}{M} K_i^E \qquad (2)$$

where W_i (t) is the mass of material coarser than size x_i inside the mill, F_i and G_i (t/h) are the cumulative mass flow-rates of material coarser than size x_i for the mill feed and product streams respectively.

A similar equation to eq. (2) can be constructed for

material coarser than x_{i+1}:

$$\frac{dW_{(i+1)}}{dt} = F_{i+1} - G_{i+1} - W_{i+1}\frac{P}{M}K^E_{i+1} \qquad (3)$$

The accumulation of material within size x_i ($i = 2, 3, ..., n-1$) is given by the difference between eq. (3) and eq. (2):

$$\frac{dw_i}{dt} = f_i - g_i w_i + \left\{ W_i\frac{P}{M}K^E_i - (w_i + W_i)\frac{P}{M}K^E_{i+1} \right\} \quad (4)$$

The mass balance for particles in the sink size class n is:

$$\frac{dw_n}{dt} = f_n - g_n w_n + W_n\frac{P}{M}K^E_n \qquad (5)$$

The water mass balance is given by:

$$\frac{dw_0}{dt} = f_0 - g_0 w_0 \qquad (6)$$

where the flow of water into the mill is f_0 (m^3/h), the hold-up of water in the mill is w_0 (m^3) and the discharge rate of water out of the mill is g_0 (h^{-1}).

The final cumulative breakage rate population balance model for the grinding mill is given by eqs. (1), (4), (5) and (6).

Cumulative Breakage Rate Function The cumulative breakage rate function can be represented by a simple equation with parameters that can be back-calculated from sampling campaign data (Austin and Klimpel, 1984; Hinde and Kalala, 2009).

At steady-state, the derivatives of eq. (1), (4) and (5) are zero and the specific cumulative breakage rate function values can be determined from the remaining variables which can be measured on a plant or pilot plant:

$$K^E_2 = \frac{f_1 - g_1 w_1}{w_1 \frac{P}{M}}$$
$$K^E_{i+1} = \frac{f_i - g_i w_i + W_i \frac{P}{M}K^E_i}{(w_i + W_i)\frac{P}{M}}; \ i = 2, 3, ..., n-1 \qquad (7)$$
$$K^E_n = \frac{f_n - g_n w_n}{w_n \frac{P}{M}}$$

Once K^E_i for all size classes ($i = 2, 3, ..., n$) has been back calculated from plant measurements, the values of K^E_i can be fitted to the following equation from Hinde and Kalala (2009):

$$\hat{K}^E_i = \kappa_1 \left(\frac{x_i^{\alpha_1}}{1 + (x_i/\mu)^\lambda} + \kappa_2 x_i^{\alpha_2} \right) \ ; \ i = 2, 3, ..., n \quad (8)$$

where κ_1, κ_2, α_1, α_2, μ and λ are model parameters to be fitted. The value of K^E_i for a specific size class (say 0.6 mm) will remain the same irrespective whether or not the size class is part of a set of 5, 9 or 25 size classes. However, the estimation of the parameters in the function above may differ depending on the size class set used and the distribution of the size class set. If 5 size classes were used to calculate the values of K^E_i, the function will be able to fit the 5 values of K^E_i. Care should be taken to interpolate from 5 size classes to 9 or more size classes. Only if there is a high degree of confidence that the distribution of the 5 size classes capture the non-linearity of the breakage rate function, can such an interpolation be made with confidence.

Discharge Rate Function The discharge rate function, which describes the rate at which slurry passes through the discharge grate, can be approximated by:

$$\begin{aligned} g_i &= g_{max} \ ; \ x_i \le x_m \\ g_i &= g_{max}\frac{\ln x_i - \ln x_g}{\ln x_m - \ln x_g} \ ; \ x_m < x_i \le x_g \\ g_i &= 0 \ ; \ x_i > x_g \end{aligned} \qquad (9)$$

where g_{max} (h^{-1}) is the specific discharge rate for water and fines up to size x_m. Size x_g is the effective mesh size of the grate above which discharge is zero.

Power Draw Function The power draw of the mill is a function of the hold-up of water, ore and grinding media in the mill. A number of models are available in literature to estimate the power draw of SAG mills (Austin, 1990; Morrell, 2004). The cumulative rates model as described in Hinde and Kalala (2009) makes use of the power draw model of Austin (1990), which will also be used in this study:

$$P = 10.6D^{2.5}L\left(1 - 1.03J_T\right)\left(1 - \frac{0.1}{2^{9-10\alpha_{speed}}}\right)\alpha_{speed}\cdot$$
$$\left[(1 - \varepsilon_c)\left(\frac{\rho_S}{w_c}\right)J_T + 0.6J_B\left(\rho_B - \frac{\rho_S}{w_c}\right) \right] \qquad (10)$$

where J_T and J_B are the static fractional volumetric filling of the mill for the total charge and for the balls respectively, ε_c is the porosity of the charge, w_c is the weight of ore expressed as a fraction of the total mass of ore and water in the mill, ρ_B and ρ_S (t/m^3) are the density of the balls and the density of the ore respectively, α_{speed} is the mill speed expressed as a fraction of the critical speed (the speed at which the material in the mill centrifuges) and D and L (m) are the internal diameter and length of the mill respectively.

The static fractional volumetric filling of the mill for the total charge J_T can be approximated by:

$$J_T = \left(\frac{w_b}{\rho_B} + \frac{M}{\rho_S} + \frac{\varepsilon_c}{1 - \varepsilon_c}\left(\frac{w_b}{\rho_B} + \frac{M}{\rho_S}\right) \right)/v_{mill} \qquad (11)$$

where w_b (t) is the mass of balls and v_{mill} (m^3) is the internal volume of the mill.

The Austin power model is based on what can be measured directly in practice. The fractional volume filling of a mill is usually expressed as the static fractional filling of the mill measured after a crash stop. If the mill is filled only with balls, it is assumed that the static porosity is around 0.4. However, if the mill is filled with a mixture of rocks, pebbles, fines and balls, some of the fines will fill the voids between the rocks, pebbles and balls to give an overall porosity that is less than 0.4. In Austins power equation for SAG mills, a default value of 0.3 is assumed. If the water is taken into consideration, after a crash stop

4

it can either partially fill the remaining voids, exactly fill the voids, or overfill the voids (slurry pooling). The model assumes that the ratio of ore solids mass to ore plus water has a default value of 0.8. Of course, under dynamic conditions the solids porosity will be much larger than the static porosity, as revealed in DEM/CFD simulations, but the technology of measuring the dynamic porosity is not well developed and that is why it customary to use the static charge levels as the independent variables in most mill power models (Hinde, 2013).

3.1.2. Sump model

The sump is treated as a perfectly mixed vessel and the residence time in the piping and hydrocyclone is assumed to be small compared to that of the sump. The accumulation of material in the sump is given by the difference in input and output flows:

$$\frac{dz_i}{dt} = r_i - s_i = r_i - \frac{CFF z_i}{v_{pulp}} \quad (12)$$

where z_i (m³) is the volume of material in size class i in the sump, r_i (m³/h) is the flow-rate of material in size class i into the sump, s_i is the flow-rate of material in size class i out of the sump, v_{pulp} (m³) is the total volume of pulp in the sump and CFF (m³/h) is the cyclone feed flow. The level to which the sump is filled with slurry is given by $SLEV$ [m].

The flow-rate of water out of the sump s_0 is given by:

$$s_0 = CFF \left(1 - \phi/100\right) \quad (13)$$

where ϕ is the volume percentage solids in the cyclone feed pulp.

3.1.3. Hydrocyclone model

The hydrocyclone model used in this study is the Plitt model (Plitt, 1976; Flintoff et al., 1987). Although this model is commonly used to model hydrocyclones, the model cannot accommodate high recoveries of solids to underflow as well as wide variations in feed size. Also, changes in the cyclone feed solids concentration and size distribution have a severe impact on the performance of the hydrocyclone model. Care should be taken when extrapolating this model outside the range of conditions used to estimate the model parameters. If the Plitt model uses parameters determined from pilot plant tests, the model cannot be guaranteed to operate correctly on industrial scale (Napier-Munn et al., 1999).

The fraction of particles in the overflow of the cyclone smaller than the specification size (usually 75 μm) is given by the product particle size estimate PSE.

4. Model Reduction

The largest size class set considered in this study to model the grinding mill circuit by means of the cumulative rates model is 25 size classes. It is assumed that 25

Table 3: Size class sets in [mm]. (l: Log-Linear Separation; c: Chosen Separation)

#	25(Ref)	9l	9c	5l	5c	3l	3c
1	307.2	307.2	307.2	307.2	307.2	307.2	307.2
2	217.2						
3	153.6			153.6			
4	108.6	108.6					
5	76.8						
6	54.3			54.3		54.3	
7	38.4	38.4	38.4	38.4			
8	27.2						
9	19.2						
10	13.6	13.6					
11	9.6						
12	6.8						
13	4.8	4.8		4.8		4.8	
14	3.4						
15	2.4						
16	1.7	1.7	1.7				
17	1.2						
18	0.85				0.85		
19	0.60	0.6	0.6	0.6			0.6
20	0.42						
21	0.30		0.3				
22	0.21	0.21			0.21		
23	0.15		0.15				
24	0.106						
25	0.075	0.075	0.075	0.075	0.075	0.075	0.075

Table 4: Breakage rate and Rosin-Rammler function parameters.

Parameter	Value	Uncertainty
κ_1	1.13	5%
κ_2	3.0e-6	5%
α_1	1.11	5%
α_2	2.55	3%
λ	1.16	5%
μ	0.33	3%
β	0.36	20%
$D_{63.2}$	41.1	20%

size classes give a more accurate representation of the ore distribution and the non-linear cumulative breakage rate function K_i^E than fewer size classes. Therefore, the cumulative rates model with 25 size classes is the reference model against which models with smaller size class sets are compared. The reference size class set is named 25(Ref).

The smallest size class considered is $x_n = 75$ μm. This is also the specification size for the product. This size class is increased 25 times by a factor of $\sqrt{2}$, the usual difference in aperture size for sieves (Stanley, 1987), until the largest size class $x_1 = 307.2$ mm is reached. The sizes in set 25(Ref) are shown in the second column of Table 3.

A large set of size classes can be reduced by lumping size classes together with a constant factor separating sizes. If size class set 25(Ref) is reduced in this manner to 9 size
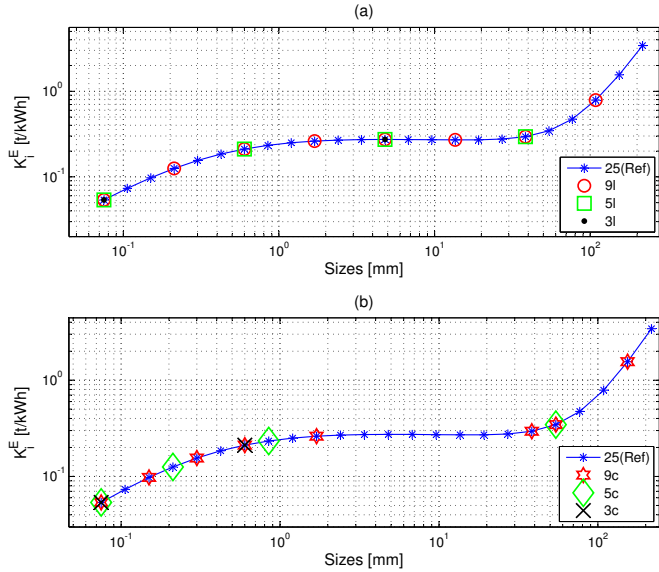
Figure 2: (a) Cumulative breakage rate function represented by the reference size class set 25(Ref) and the reduced size class sets $9l$, $5l$ and $3l$. The sizes in the latter three sets are distributed log-linearly. (b) Cumulative breakage rate function represented by the reference size class set 25(Ref) and the reduced size class sets $9c$, $5c$ and $3c$. The sizes in the latter three sets were chosen to best represent the non-linearity of the curve $\log\left(K_i^E\right)$.

classes where the largest size remains $x_1 = 307.2$ mm and the smallest $x_n = 75$ μm, the sizes differ by a factor of $(\sqrt{2})^3$. For 5 size classes the sizes differ by $(\sqrt{2})^6$, and for 3 size classes by $(\sqrt{2})^{12}$. These three reduced size class sets are shown in Table 3 and are called $9l$, $5l$ and $3l$ respectively. The l indicates that the sizes in the reduced sets are log-linearly distributed.

The sampling campaign in the optimisation study of Hinde (2009) used a sink size class of 38 μm. Because the study described in this paper aims to compare the product particle size estimate (PSE) for various size class sets, the product specification size class of 75 μm should appear in each size class set. The simplest way to achieve this is to use a sink size class of 75 μm. If the sink size class is 38 μm and the reference set of 25 size classes is reduced to 9 or 5 size classes log-linearly distributed, the 75 μm size class would fall away and the PSE would have to be determined by interpolation which is not advisable.

The parameter values for the breakage rate function in eq. (8) are shown in Table 4 . These parameter values were estimated in an optimisation study based on the cumulative rates model of an industrial plant (Hinde, 2009). The cumulative breakage rate function K_i^E in eq. (8) represented by the three aforementioned size class sets is shown in Fig. 2a. From this figure it can be seen that size class sets $5l$ and $3l$ do not capture the non-linearity of $\log(K_i^E)$ below size 0.85 mm and above size 38.4 mm. Since K_1^E is undefined (see eq. (1)), only $n-1$ points appear in Fig. 2 when K_i^E is represented with n size classes.

In terms of the variable rates model described in Apelt

et al. (2002), a plot of the breakage rate of ore r_i (defined as the breakage rate for particles in size class x_i) for all size classes will usually produce a dip at the critical size range for a ROM ore SAG mill with a high ball load (Napier-Munn et al., 1999). This dip is not apparent in Fig. 2 because K_i^E is defined differently - it is the cumulative breakage rate of particles above size x_i to below that size.

The sizes in the reduced size class sets do not need to be log-linearly distributed. Reduced size class sets can be specified in such a way that the shape of K_i^E remains well defined by the sizes in the size class sets excluding the largest size x_1. Thus, three new reduced size class sets of 9, 5 and 3 sizes are chosen such that the non-linear nature of the breakage rate function is captured as best possible. The sizes in these three sets are chosen from the sizes in the reference set 25(Ref). The breakage rate function rather than the distribution of the mill charge is used to choose the smaller size class sets. The mill charge is a function of the breakage rate function and will reflect the shape of the breakage rate function. The three new reduced size class sets are shown in Table 3 and are called $9c$, $5c$ and $3c$. The c indicates that the size classes where chosen to best fit K_i^E. The procedure to choose these sizes is described below.

The reference size class set 25(Ref) consists of $N = 25$ size classes and is represented by $X = \{307.2, 217.2, ..., 0.075\}$ mm. For the reduced size class set S of M sizes, the largest size class is $x_1 = s_1 = 307.2$ mm and the smallest is $x_{25} = s_M = 75$ μm. Thus, there remains $M - 2$ sizes to choose from set X to complete set S. The set m contains the size class numbers from set X included in the reduced size class set S, e.g. if $M = 3$, then $m = \{1, 19, 25\}$ and $S = \{307.2, 0.6, 0.075\}$ mm. The function f below determines the squared sum of the distances between the curve $\log(K_i^E)$ represented by the 25 size classes in set X and straight lines connecting the points on $\log(K_i^E)$ represented by the M size classes in set S. In other words, function f determines the distance between $\log(K_i^E)$ represented by set X and the straight line approximation of $\log(K_i^E)$ with $M-1$ lines. The combination of sizes that gives the minimum value of function f is regarded as the best representation of K_i^E by M size classes:

$$
\begin{aligned}
f = &\sum_{j=2}^{M-1} \sum_{i=m(j)+1}^{m(j+1)-1} [\log K_i^E - \log K_{m(j+1)}^E \\
&- \frac{\log K_{m(j)}^E - \log K_{m(j+1)}^E}{X_{m(j)} - X_{m(j+1)}} \left(X_i - X_{m(j+1)}\right)]^2 \\
&+ \sum_{k=3}^{m(2)-1} [\log K_k^E - \log K_{m(2)}^E \\
&- \frac{\log K_2^E - \log K_{m(2)}^E}{X_2 - X_{m(2)}} \left(X_k - X_{m(2)}\right)]^2
\end{aligned}
\tag{14}
$$

The representation of the breakage rate function by size class sets $9c$, $5c$ and $3c$ is shown in Fig. 2b.

5. System Identification

The seven size class sets shown in Table 3 are used to create seven non-linear cumulative rates models. These

Table 5: Grinding mill circuit parameters.

Parameter	Description	Value	Unit
α_c	Fraction of critical mill speed	0.71	-
D	Internal mill diameter	4.20	m
ε_c	Effective static porosity of the charge	0.3	-
g_{max}	Specific discharge rate for water and fines	27.5	h^{-1}
J_B	Static fractional volumetric filling of the mill for balls	0.24	-
L	Internal mill length	4.27	m
ρ_s	Ore density	3.2	t/m^3
ρ_b	Ball density	7.85	t/m^3
v_{mill}	Mill internal volume	59.12	m^3
w_b	Ball mass in the mill	66.8	t
x_g	Effective mesh size of grate for zero discharge	12	mm
x_m	Maximum fines size in discharge rate function	1	mm

Table 6: Operating point, variable constraints and MPC weights.

Variable	Min	Max	OP	Weight	Unit
Manipulated Variables					
CFF	100	450	288	1.8e-7	m^3/h
MFS	0	150	69	1.0e-6	t/h
SFW	0	200	90	5.6e-7	m^3/h
MIW	0	20	3.7	5.6e-3	m^3/h
Controlled Variables					
PSE	0.5	0.85	0.69	1.75	Fraction
JT	0.2	0.5	0.32	8.3e-2	Fraction
$SLEV$	0.2	2	0.92	1	m
P_{mill}	-	-	1095	-	kW

Figure 3: Cumulative distribution for solids feed, mill charge and sump charge represented by 25, 9, 5 and 3 size classes. (Ref - the reference size class set, l - size classes are log-linearly separated, c - separation between size classes is chosen.

The cumulative distribution of the solids feed and the cumulative distributions of the hold-up of ore in the mill and sump during linearization are shown in Fig. 3. The cumulative distribution of the solids feed to the mill as measured during the optimisation study of Hinde (2009) was fitted to the truncated Rosin-Rammler distribution function:

$$P_{RR}(\bar{x}) = 1 - \exp\left(-\left(\frac{\eta}{\eta_{63.2}}\right)^{\beta}\right) \quad (15)$$

where $\eta = \frac{\varepsilon}{1-\varepsilon}$ and $\varepsilon = \bar{x}/x_1$. The largest size class is given by x_1, the vector containing all size classes from 1 to 25 is $\bar{x}$ and the measure of the spread in particle sizes is given by β. The size $D_{63.2}$ is the size where the cumulative distribution of solids feed is at 63.2% of its maximum; therefore $\eta_{63.2} = \frac{D_{63.2}/x_1}{1-D_{63.2}/x_1}$. The parameter values for this function are shown in Table 4. These parameter values were determined by fitting the Rosin-Rammler equation to the feed size distribution data from the report of Hinde (2009).

5.2. Linearized models

The System Identification Toolbox[1] in MATLAB was used to linearize the non-linear cumulative rates model for each of the seven different size class sets. The 7 non-linear models, each based on a different size class set, were fitted to the 12 elements in the linear transfer function matrix below. The same data set consisting of randomized steps in the manipulated variables of 10 h each for 120 h around

non-linear models are all linearized around the same operating point by means of a standard system identification procedure (Soderstrom and Stoica, 1989). The seven linear models are used to design seven separate linear model predictive controllers to control the grinding mill circuit shown in Fig. 1 as represented by the non-linear cumulative rates containing the reference set of 25 size classes. The performance of each controller should give an indication of the accuracy of the model used to design the controller.

5.1. Parameter values and operating point

The grinding mill circuit parameter values are shown in Table 5. The operating point of the circuit during linearization is shown in Table 6. The empirical model parameters and circuit's operating point used in this study were determined from an industrial scale plant during the optimisation study of Hinde (2009).
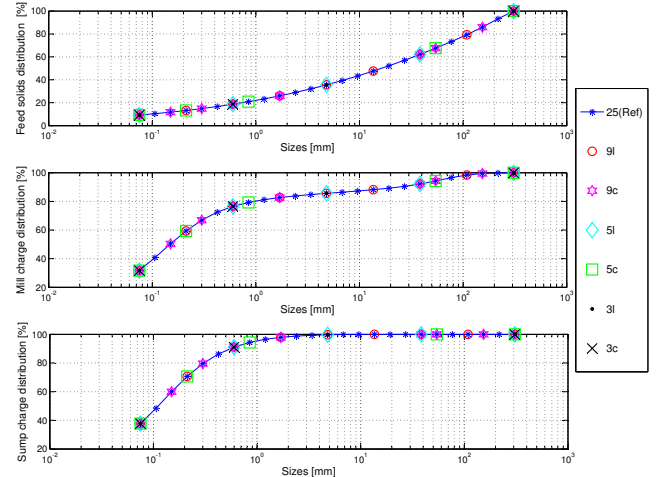
---

[1]System Identification Toolbox^{TM} is a registered trademark of The Mathworks, Inc.

the operating point of the circuit was used to identify the different linear models.

$$\begin{bmatrix} PSE \\ JT \\ SLEV \end{bmatrix} = \begin{bmatrix} G_{11} & G_{12} & G_{13} & G_{14} \\ G_{21} & G_{22} & G_{23} & G_{24} \\ G_{31} & G_{32} & G_{33} & G_{34} \end{bmatrix} \begin{bmatrix} CFF \\ MFS \\ SFW \\ MIW \end{bmatrix} \quad (16)$$

The transfer function element G_{11} in eq. (16) has the form:

$$G_{11} = \frac{K_{11}(sT_{z_{11}}+1)}{(sT_{p1_{11}}+1)(sT_{p2_{11}}+1)}e^{-T_{d_{11}}s} \quad (17)$$

The transfer function elements $G_{12-14,21,23,24}$ have the form:

$$G_{ij} = \frac{K_{ij}}{sT_{p_{ij}}+1}e^{-T_{d_{ij}}s} \quad (18)$$

The transfer function element G_{22} has the form:

$$G_{22} = \frac{K_{22}}{sT_{p_{22}}+1} \quad (19)$$

The transfer function elements $G_{31,33}$ have the form:

$$G_{ij} = \frac{K_{ij}}{s} \quad (20)$$

The transfer function elements $G_{32,34}$ have the form:

$$G_{ij} = \frac{K_{ij}}{s}e^{-T_{d_{ij}}s} \quad (21)$$

For the equations above, K_{ij} is a proportional gain, $T_{d_{ij}}$ is a time delay, $T_{p_{ij}}$ is a pole time constant and $T_{z_{ij}}$ is a zero time constant.

The difference in the model parameter values shown in Table 7 are as a result of the different number of size classes from which these models were derived. Tables 7 and 8 show the values of the transfer function parameters for the log-linear and the chosen size class set distributions respectively. The time delays and the time constants are given in hours. The linearized model of the circuit modelled with 25 size classes is regarded as the reference model.

Table 7 show very little difference between the transfer function parameter values for reference set 25(Ref) and size class set $9l$. A larger difference in transfer function parameter values occurs between size class set 25(Ref) and size class set $5l$. For Table 8 the difference between the transfer function parameter values for set 25(Ref) and size class sets $9c$ and $5c$ are relatively small.

The fit of the transfer function G_{11} in eq. (17) to the response of the circuit modelled with size class set $3l$ produced a transfer function that responded too slow to capture the dynamics between CFF and PSE. A first order plus time delay transfer function provided a better fit and was therefore used for the linearized model of size class set $3l$. As shown in Table 7, the gains of the linearized model for set $3l$ are all in the correct directions, but differ significantly in magnitude from the gains of the model for

Table 7: Transfer function parameters of log-linearly distributed size class sets.

Function		Size class set			
PSE		25(Ref)	$9l$	$5l$	$3l$
	K_{11}	-1.7e-3	-1.7e-3	-2.2e-3	-3.4e-3
G_{11}	$T_{p1_{11}}$	0.84	0.87	0.89	2.4
-	$T_{p2_{11}}$	4.3e-2	5.5e-4	0.3	-
CFF	$T_{z_{11}}$	-0.16	-0.19	-0.05	-
	$T_{d_{11}}$	0.01	0.01	0.01	0.01
G_{12}	K_{12}	-3.7e-3	-3.8e-3	-4.4e-3	-5.5e-3
-	$T_{p_{12}}$	0.76	0.75	0.74	1.9
MFS	$T_{d_{12}}$	0.05	0.05	0.05	0.05
G_{13}	K_{13}	4.0e-3	4.1e-3	5.2e-3	8.9e-3
-	$T_{p_{13}}$	0.96	0.97	0.96	2.8
SFW	$T_{d_{13}}$	0.01	0.01	0.01	0.01
G_{14}	K_{14}	4.1e-3	4.2e-3	5.4e-3	0.01
-	$T_{p_{14}}$	0.41	0.40	0.35	2.0
MIW	$T_{d_{14}}$	0.02	0.02	0.02	0.02
JT		25(Ref)	$9l$	$5l$	$3l$
G_{21}	K_{21}	5.0e-4	5.1e-4	5.3e-4	2.1e-3
-	$T_{p_{21}}$	0.27	0.28	0.24	1.4
CFF	$T_{d_{21}}$	0.01	0.01	0.01	0.01
G_{22}	K_{22}	1.1e-3	1.1e-3	1.1e-3	3.3e-3
MFS	$T_{p_{22}}$	0.30	0.29	0.26	1.2
G_{23}	K_{23}	-5.1e-4	-5.1e-4	-4.6e-4	-2.1e-3
-	$T_{p_{23}}$	0.91	0.93	1.1	1.4
SFW	$T_{d_{23}}$	0.02	0.02	0.02	0.02
G_{24}	K_{24}	-5.3e-4	-5.4e-4	-4.8e-4	-2.6e-3
-	$T_{p_{24}}$	0.39	0.40	0.44	1.3
MIW	$T_{d_{24}}$	0.05	0.05	0.05	0.05
$SLEV$		25(Ref)	$9l$	$5l$	$3l$
G_{31}	K_{31}	-0.13	-0.13	-0.13	-0.12
G_{32}	K_{32}	0.11	0.11	0.11	0.11
MFS	$T_{d_{32}}$	0.1	0.1	0.1	0.1
G_{33}	K_{33}	0.25	0.25	0.25	0.23
G_{34}	K_{34}	0.25	0.25	0.25	0.23
MIW	$T_{d_{34}}$	0.04	0.04	0.04	0.04

the reference set 25(Ref). In contrast to set $3l$, the difference in transfer function parameter values between the linear model of set 25(Ref) and the linear model of set $3c$ is much smaller.

For the sump level $SLEV$, the transfer function parameter values are almost identical irrespective of the size class set.

6. Model Predictive Control

The control objectives for a grinding mill circuit are to improve the quality of the product (by increasing the fineness of the grind or reducing the product size fluctuations), to maximise the throughput, to decrease the power consumption, to reduce the usage of grinding media such as balls and to improve process stability. These objectives are

Table 8: Transfer function parameters of chosen size class sets.

Function		25(Ref)	9c	5c	3c
PSE					
G_{11}	K_{11}	-1.7e-3	-1.7e-3	-1.7e-3	-2.1e-3
-	$T_{p1_{11}}$	0.84	0.80	0.81	0.81
-	$T_{p2_{11}}$	4.3e-2	4.4e-4	6.3e-4	0.27
CFF	$T_{z_{11}}$	-0.16	-0.17	-0.18	-0.06
	$T_{d_{11}}$	0.01	0.01	0.01	0.01
G_{12}	K_{12}	-3.7e-3	-3.8e-3	-3.8e-3	-4.4e-3
-	$T_{p_{12}}$	0.76	0.65	0.67	0.61
MFS	$T_{d_{12}}$	0.05	0.05	0.05	0.05
G_{13}	K_{13}	4.0e-3	4.0e-3	4.0e-3	5.1e-3
-	$T_{p_{13}}$	0.96	0.85	0.88	0.77
SFW	$T_{d_{13}}$	0.01	0.01	0.01	0.01
G_{14}	K_{14}	4.1e-3	4.1e-3	4.1e-3	5.3e-3
-	$T_{p_{14}}$	0.41	0.34	0.27	0.28
MIW	$T_{d_{14}}$	0.02	0.02	0.02	0.02
JT		25(Ref)	9c	5c	3c
G_{21}	K_{21}	5.0e-4	5.1e-4	5.3e-4	5.4e-4
-	$T_{p_{21}}$	0.27	0.30	0.33	0.32
CFF	$T_{d_{21}}$	0.01	0.01	0.01	0.01
G_{22}	K_{22}	1.1e-3	1.1e-3	1.2e-3	1.2e-3
MFS	$T_{p_{22}}$	0.30	0.26	0.26	0.23
G_{23}	K_{23}	-5.1e-4	-5.1e-4	-5.3e-4	-4.4e-4
-	$T_{p_{23}}$	0.91	0.80	0.80	0.98
SFW	$T_{d_{23}}$	0.02	0.02	0.02	0.02
G_{24}	K_{24}	-5.3e-4	-5.3e-4	-5.5e-4	-4.7e-4
-	$T_{p_{24}}$	0.39	0.34	0.31	0.32
MIW	$T_{d_{24}}$	0.05	0.05	0.05	0.05
SLEV		25(Ref)	9c	5c	3c
G_{31}	K_{31}	-0.13	-0.13	-0.13	-0.13
G_{32}	K_{32}	0.11	0.11	0.11	0.11
MFS	$T_{d_{32}}$	0.1	0.1	0.1	0.1
G_{33}	K_{33}	0.25	0.25	0.25	0.25
G_{34}	K_{34}	0.25	0.25	0.25	0.25
MIW	$T_{d_{34}}$	0.04	0.04	0.04	0.04

interrelated and necessitates trade-offs to be made (Craig and MacLeod, 1995).

The main challenges when controlling a grinding process are the strong coupling between variables, the existence of large time delays, the variation of parameters over time and the non-linearities in the process. Model Predictive Control (MPC) is ideal for the grinding process because it has the ability to handle pairing problems in multivariable systems, to handle processes with large time delays and to impose constraints on manipulated and controlled variables. The disadvantages of an MPC scheme are the computational burden for large processes with long control and prediction horizons, the dependency on a reliable and accurate process model and the deterioration in controller performance in the presence of strong external disturbances (Chen et al., 2009).

The study of Ramasamy et al. (2005) indicated improvements in the performance of a laboratory grinding mill circuit controlled by means of a MPC scheme compared to a multi-loop detuned PI(D) control scheme. MPC has also been successfully used to control industrial grinding mill circuits (Chen et al., 2007, 2008; Wei and Craig, 2009). A survey of commercial MPC technologies can be found in Qin and Badgwell (2003).

6.1. Overview

A linear MPC scheme is a model-based control strategy that utilizes a linear model of the plant to predict future behaviour of the plant. At each sampling interval the controller attempts to calculate a series of C control moves that will optimize the future behaviour of the plant for the next P sampling intervals. Because a new series of control moves is calculated at every sampling interval, only the first control move in the series is implemented. A performance index defines the optimal future behaviour of the plant and aims to prevent violations of manipulated and controlled variable constraints, to prevent excessive manipulated variable changes and to drive controlled variables to their optimal set-points (Qin and Badgwell, 2003).

The control action taken at time k is obtained by selecting an input sequence u that minimizes the scalar performance index J:

$$J(k) = \sum_{j=1}^{P} \left[\hat{y}(k+j) - r(k+j) \right]^T Q \left[\hat{y}(k+j) - r(k+j) \right]$$
$$+ \sum_{j=1}^{C} \left[\Delta u(k+j-1) \right]^T R \left[\Delta u(k+j-1) \right]$$
$$(22)$$

where $\hat{y}(k)$, $r(k)$ and $\Delta u(k)$ are the vectors of predicted outputs, set-point trajectories and changes in the inputs at time k respectively, P and C are the prediction and control horizon respectively, $Q = \text{diag}\,[q_1, q_2...q_P]$ and $R = \text{diag}\,[r_1, r_2...r_C]$ are the error and input weighting matrices respectively. The magnitude and rate constraints on the manipulated and controlled variables are given by:

$$u_{\min} \leq u(k) \leq u_{\max}, \quad k = 0, 1, ...C - 1$$
$$\Delta u_{\min} \leq \Delta u(k) \leq \Delta u_{\max}, \quad k = 0, 1, ...C - 1 \quad (23)$$
$$y_{\min} \leq y(k) \leq y_{\max}, \quad k = 0, 1, ..., P - 1$$

Tighter control of controlled variables can be achieved by choosing larger weights in matrix Q and excessive variations in manipulated variables can be avoided by choosing appropriate values for matrix R (Chen et al., 2007, 2008).

6.2. Controller design

The Model Predictive Control Toolbox[2] of MATLAB was used to create seven controllers from the seven linearised plant models of the grinding mill circuit. All seven controllers use a sampling time of 10 s, a prediction horizon of 200 samples and a control horizon of 3 samples. The constraints imposed by the controller for each variable and the weights for the R and Q matrices in eq. (22)

---

[2]Model Predictive Control Toolbox^{TM} is a registered trademark of The Mathworks, Inc.

are shown in Table 6. The weighting matrices, calculated during the tuning of the controller, are shown below for further clarification:

$$Q = \text{diag}\,[1.75, 0.083, 1]$$
$$R = \text{diag}\,[1.8\text{e-}7, 1.0\text{e-}6, 5.6\text{e-}7, 5.6\text{e-}3] \quad (24)$$

It is important to note that the relative values of the Q and R weighting matrices and not the absolute values of these matrices determine the performance of the controller. Because the inputs and outputs of the models have not been scaled, the weights have been scaled according to the ranges of the manipulated variables. The controller aims to control PSE tightly, while allowing JT and $SLEV$ to vary around their set-points and within their constraints. It is important to maintain JT and $SLEV$ within their constraints as these variables are open loop unstable. The controller makes equal use of CFF, MFS and SFW, but less use of MIW to drive the controlled variables to their set-points.

7. Simulation, Results and Discussion

7.1. Simulation

A simulation platform was created in Simulink[3] to simulate the single-stage grinding mill circuit in Fig. 1 modelled by the non-linear cumulative rates model with 25 size classes. Each one of the seven model predictive controllers was implemented on the non-linear model. Therefore, there are seven simulations where each simulation makes use of a different controller to control the non-linear model with 25 size classes. The performance of the controllers based on the reduced size class sets is compared to the performance of the controller based on the reference size class set of 25 sizes.

The equilibrium of a grinding mill is perturbed when the feed-rate, feed ore distribution and hardness varies. The effect of these variations on the behaviour of the grinding mill requires time to decay. Although it is desirable to manipulate all three of these variables, only feed-rate can be manipulated. A grinding mill circuit has to contend with the other two variables as disturbances (Olivier et al., 2012). Changes in the feed hardness and size distribution will result in changes in the grinding media size distribution, which will affect the breakage characteristics in the mill (Napier-Munn et al., 1999; Coetzee et al., 2010).

During simulation, the feed ore distribution was altered every 13 h by adjusting the Rosin-Rammler function parameters in eq. (15). The feed ore hardness was altered indirectly by adjusting the breakage rate function parameters in eq. (8) every 8 h. The parameters in both functions were randomly varied according to a uniform distribution where the minimum and maximum of the distribution are given by:

$$\min = p(1 - \Delta_p/100); \quad \max = p(1 + \Delta_p/100) \quad (25)$$

---

[3]Simulink is a registered trademarks of The MathWorks Inc.
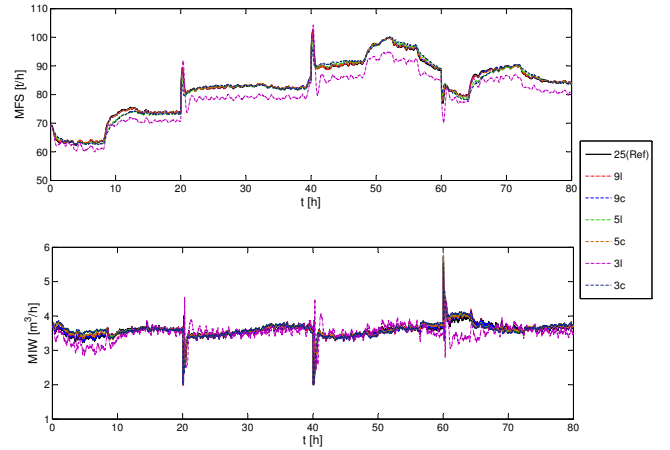

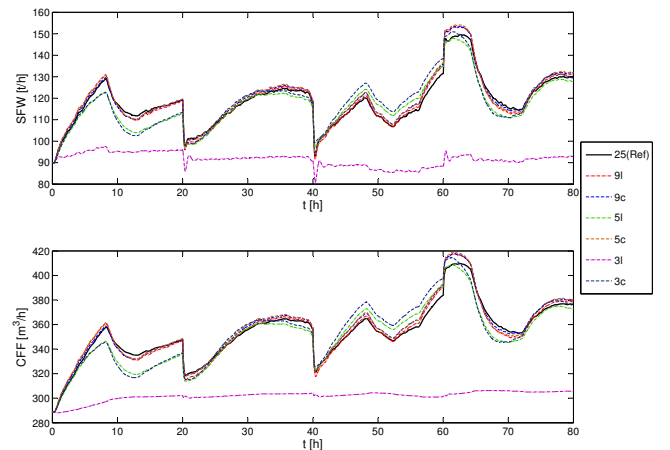Figure 4: Manipulated variables MFS and MIW for each controller of the seven size class sets shown in Table 3.

Figure 5: Manipulated variables SFW and CFF for each controller of the seven size class sets shown in Table 3.

where Δ is the uncertainty of parameter p. The uncertainties for the parameters in both functions can be seen in Table 4.

Measurement noise was added to variables PSE, JT and $SLEV$. The noise was normally distributed with a variance of 2% for $SLEV$ and a variance of 3% for PSE and JT. Given the ranges of the three controlled variables, the noise on PSE and JT is significantly larger than the noise on $SLEV$.

During simulation, the set-points for JT and $SLEV$ were kept constant. The set-point for PSE was adjusted every 20 h: $PSE = \{0.69, 0.64, 0.58, 0.62\}$.

7.2. Results and Discussion

The manipulated variables are shown in Figs. 4 and 5. All the controllers, except the controller based on size class set $3l$, adjusted the manipulated variables at similar rates and degrees of magnitude.

The fraction of the mill filled (JT) is shown in Fig. 6, the sump level ($SLEV$) is shown in Fig. 7, the fraction of
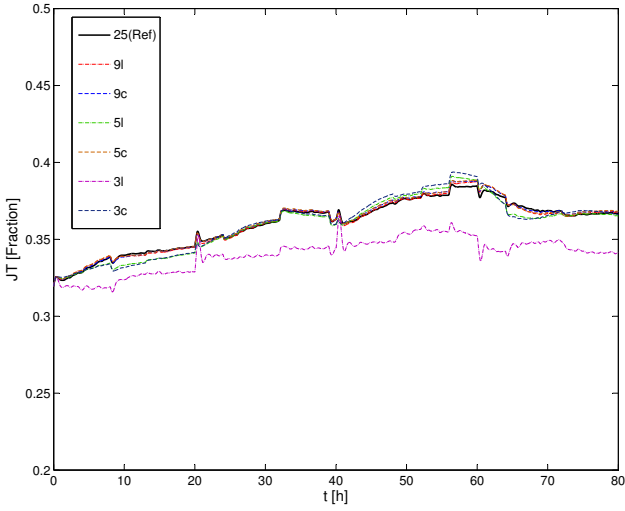
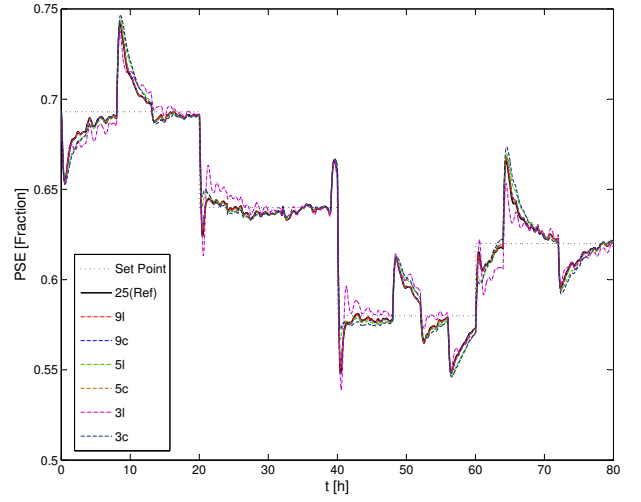Figure 6: Simulation results of fractional volumetric filling (JT) of the mill for all size class sets.

Figure 8: Simulation results of fraction of cyclone overflow that passes 75 μm (PSE) for all size class sets.
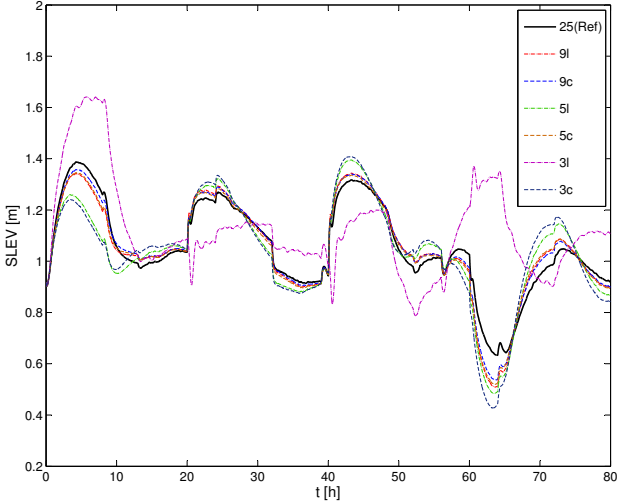

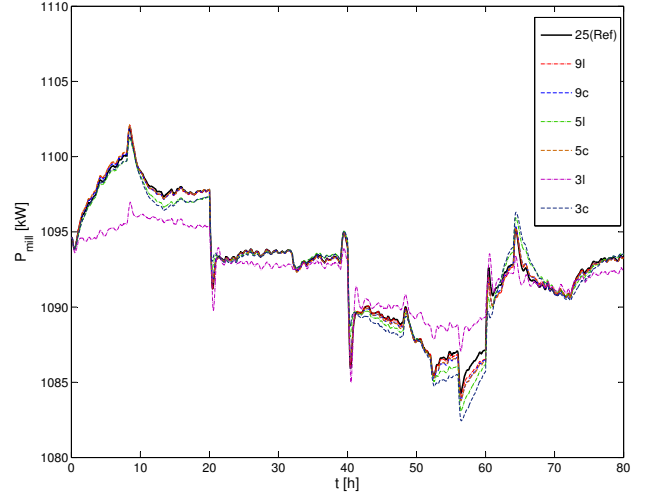Figure 7: Simulation results of sump level ($SLEV$) for all size class sets.

Figure 9: Simulation results of mill power draw (P_{mill}) for all size class sets.

the cyclone overflow that passes 75 μm (PSE) is shown in Fig. 8, and the mill power draw is shown in Fig. 9. The figures indicate that the controller allowed JT and $SLEV$ to vary within their constraints in order to have tight control of PSE. Neither JT nor $SLEV$ violates its constraints.

Figures 6 to 9 show that the controllers based on reduced size class sets $9l$, $9c$ and $5c$ cause the controlled variables to follow almost the same path as the controlled variables for the controller based on the reference size class set 25(Ref). This is to be expected since the linearized models for sets 25(Ref), $9l$, $9c$ and $5c$ have almost identical transfer function parameter values.

Although the controllers based on reduced size class sets $5l$ and $3c$ do not cause the controlled variables to follow the exact same path as the controlled variables for the

controller based on set 25(Ref), the rate and magnitude of changes remain similar. The figures indicate that controllers based on $5l$ and $3c$ are almost identical, which is too be expected since the linearized model parameters for these size class sets in Tables 7 and 8 are almost identical.

The controller based on size class set $3l$ does not cause the controlled variables JT and $SLEV$ to follow a similar path as the other controllers. Because PSE was given a high priority, the controller for set $3l$ is able control PSE in an almost identical fashion to the reference controller for set 25(Ref).

During the simulation, the feed ore hardness varies at intervals of 8 h and the feed ore distribution at intervals of 13 h. The first disturbance occurs at time 0 h, as seen in Fig. 8. This figure shows that the controller is not able to suppress large disturbances very quickly. The disturbances
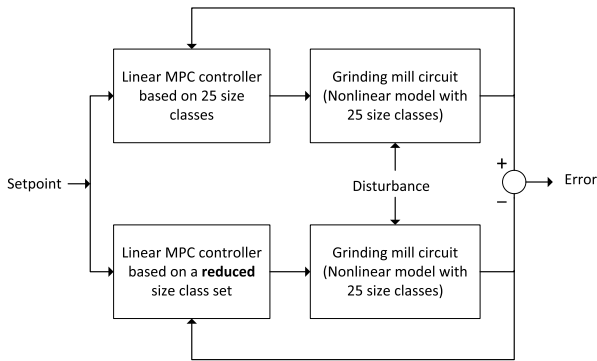
11

Figure 10: Illustration of simulation structure.

Table 9: Percentage NRMSE between reference model and reduced models' controlled and manipulated variables.

	$9l$	$9c$	$5l$	$5c$	$3l$	$3c$
CFF	13.9	15.0	36.1	17.8	251	43.9
MFS	2.25	3.15	10.4	3.24	39.5	13.7
SFW	14.2	15.7	36.6	18.4	257	44.1
MIW	17.6	20.1	53.2	33.9	107	64.5
PSE	0.91	1.95	8.01	1.73	12.9	10.4
JT	7.80	8.45	21.8	9.83	133	27.5
$SLEV$	23.9	18.9	44.1	23.0	120	55.2
P_{mill}	5.25	6.38	15.4	6.87	45.5	21.9

cause a mismatch between the plant and the model used by the controller (Olivier and Craig, 2013). However, the controller is able to return PSE back to its set-point in the presence of the disturbances. It should be remembered that the size of the sump has an influence on the ability to reject disturbances in PSE. A large sump acts as a large buffer and provides more leeway to reject disturbances.

The analysis of the performance of the controllers is illustrated in Fig. 10. The difference between the controlled or manipulated variables of the circuit with the reference size class set controller and the same variables of the circuit with a reduced size class set controller can be quantified by means of the normalised root mean squared error (NRMSE) expressed as a percentage:

$$\%NRMSE = 100 \left(\frac{\left\| y_{25(Ref)} - \hat{y} \right\|_2}{\left\| y_{25(Ref)} - mean(y_{25(Ref)}) \right\|_2} \right)$$
(26)

where $y_{25(Ref)}$ is a time-signal for the reference size class set and $\hat{y}$ is a time-signal for a reduced size class set. The results of the comparison between signal 25(Ref) and the other signals in each of the Figures 4-9 are shown in Table 9.

Table 9 affirms that the controllers for sets $9l$, $9c$ and $5c$ give approximately equal responses. These sets give a fairly accurate description of the grinding mill circuit

modelled by 25 size classes. According to the table, the controller for set $5l$ is slightly more accurate than the controller for set $3c$. These two sets define models which are reasonably similar to the model of the grinding mill circuit with the reference set. Finally, set $3l$ cannot describe the grinding mill circuit as accurately as 25 size classes. Yet, because this set correctly indicates the direction each variable will change, the linear controller for this set is able to provide reasonable control for the non-linear circuit modelled by 25 size classes.

8. Conclusion

Whereas a model with a large size class set provides valuable information for plant design and scale-up, a model with a small size class set may be more suited for process control. When modelling a grinding mill circuit, it is important to clearly identify the aim of the model.

Simulating a model with only a few size classes presents a much smaller computational burden than simulating the model with large size class set. This is because less size classes require less differential equations to be solved. Thus, the minimization of the cost function in MPC schemes should take less time because less time is necessary to predict the future behaviour of the plant with the model. An example of a robust nonlinear MPC framework with a reduced size class set can be found in Coetzee et al. (2010). Even though a reduced size class set was used, the computational time was too long for the controller to be implemented on a plant in real-time. Yet, future processors should be able to easily deal with nonlinear models with large size class sets since computational power should increase according to Moore's law.

If only a few size classes are used to characterize the inflow and outflow of each unit in the milling circuit, less sieves are required during a sampling campaign to obtain data to fit a model for process control. Since a subset of available standard sieves can be used, it is not necessary to construct special sieves for such a sampling campaign. Although this will reduce the sampling campaign time, it is possible that the sieves will not be able to handle the weight of slurry samples. A sampling campaign with only a few sieves will require careful planning to make sure that a representative slurry sample is used which the sieves will be able to handle.

When estimating the parameters of the cumulative breakage rate function it is not necessary to use 25 size classes. As seen from the linearized models, when the cumulative breakage rate K_i^E is represented by a reduced size class set the linear model of the grinding mill circuit remains almost as accurate as the linear model based on the full size class set. With fewer size classes calculation of the parameters in eq. (8) can be done more easily since more degrees of freedom are available to fit the function. However, if only a few size classes are used more care should be taken to make sure that the size class set captures the

non-linear behaviour of K_i^E. Otherwise it is not recommended to interpolate the breakage rate function from 5 size classes to 9 or more size classes.

Model accuracy does not necessarily depend on the number of size classes, but rather on their distribution. The cumulative rates model with 3 (or 5) size classes chosen according to the shape of the curve $\log K_i^E$, produced the same response as the cumulative rates model with 5 (or 9) size classes log-linearly distributed. (In other words, sets $3c$ and $5l$, and sets $5c$ and $9l$ produce similar model responses.)

Even when a model can only give an estimate of the directions of changes in the controlled variables for changes in the manipulated variables, the model can still prove useful for control purposes. The grinding mill circuit modelled with 3 size classes log-linearly distributed produced responses in the correct directions, but with incorrect magnitudes. Even though there was considerable mismatch between the plant model and the controller model, MPC was able to control PSE and maintain the other controlled variables within their constraints. Results achieved in this paper indicate that an MPC controller, which is designed based on a simple plant model, can potentially control grinding circuits with relatively large disturbances, large parameter variations and considerable model-plant mismatch.

Acknowledgement

References

Amestica, R., Gonzalez, G. D., Barria, J., Magne, L., Menacho, J., Castro, O., 1993. A SAG mill circuit dynamic simulator based on a simplified mechanistic model. XVIII International Mineral Processing Congress Sydney, 117–129.

Amestica, R., Gonzalez, G. D., Menacho, J., Barria, J., March 1996. A mechanistic state equation model for semiautogenous mills. Int. J. Mineral Process. 44-45 (SPEC. ISS.), 349 – 360.

Apelt, T. A., Asprey, S. P., Thornhill, N. F., Sept. 2002. Inferential measurement of SAG mill parameters II: State estimation. Minerals Eng. 15 (12), 1043–1053.

Austin, L. G., 1990. Mill power equation for SAG mills. Minerals Metallurgical Process. 7 (1), 57–63.

Austin, L. G., Klimpel, R. R., 1984. The back-calculation of specific rates of breakage from continuous mill data. Powder Technol. 38 (1), 77–91.

Austin, L. G., Sutherland, D. N., Gottlieb, P., 1993. An analysis of SAG mill grinding and liberation tests. Minerals Eng. 6 (5), 491–507.

Bascur, O. A., Herbst, J. A., 1985. Dynamic simulator for training personnel in the control of grinding and flotation systems. In: Proceedings 5th IFAC Symposium Mining Metallurgy, Brisbane, Australia. pp. 307–316.

Chen, X., Li, Q., Fei, S., Aug. 2008. Constrained model predictive control in ball mill grinding process. Powder Technol. 186 (1), 31 – 39.

Chen, X., Yang, J., Li, S., Li, Q., 2009. Disturbance observer based multi-variable control of ball mill grinding circuits. J. Process Control 19 (7), 1205 – 1213.

Chen, X., Zhai, J., Li, S., Li, Q., Sept. 2007. Application of model predictive control in ball mill grinding circuit. Minerals Eng. 20 (11), 1099 – 1108.

Coetzee, L. C., Craig, I. K., Kerrigan, E. C., January 2010. Robust nonlinear model predictive control of a run-of-mine ore milling circuit. IEEE Trans. Control Syst. Technol. 18 (1), 222–229.

Craig, I. K., MacLeod, I. M., May 1995. Specification framework for robust control of a run-of-mine ore milling circuit. Control Eng. Practice 3 (5), 621–630.

Flintoff, B. C., Plitt, L. R., Turak, A. A., 1987. Cyclone modelling: a review of present technology. CIM Bulletin 80 (905), 39–50.

Hinde, A. L., 2009. External Report (Confidential). Tech. rep., Mintek.

Hinde, A. L., April 2013. Private communication.

Hinde, A. L., Kalala, J. T., April 2009. The application of a simplified approach to modelling tumbling mills, stirred media mills and HPGR's. Minerals Eng. 22 (7-8), 633–641.

Hinde, A. L., Pearson, C., 2001. Conversion of primary run-of-mine ball mills at Impala Platinum Limited to fully autogenous mills. In: Proceedings SAG 2001, vol. 3, Dept. Mining Engineering, University of British Columbia, Vancouver BC, Canada. pp. 63–82.

le Roux, J. D., Craig, I. K., Hulbert, D. G., Hinde, A. L., 2013. Analysis and validation of a run-of-mine ore grinding mill circuit model for process control. Minerals Eng. 43-44, 121–134.

Morrell, S., March 2004. A new autogenous and semi-autogenous mill model for scale-up, design and optimisation. Minerals Eng. 17 (3), 437–445.

Napier-Munn, T. J., Morrell, S., Morrison, R. D., Kojovic, T., 1999. Mineral Communition Circuits: Their Operation and Optimisation, 2nd Edition. JKMRC Monograph Series in Mining and Mineral Processing.

Olivier, L., Craig, I., 2013. Model-plant mismatch detection and model update for a run-of-mine ore milling circuit under model predictive control. Journal Process Control 23 (2), 100–107.

Olivier, L., Craig, I., Chen, Y., 2012. Fractional order and bico disturbance observers for a run-of-mine ore milling circuit. Journal Process Control 22 (1), 3–10.

Plitt, L. R., 1976. A mathematical model of the hydrocyclone classifier. CIM Bulletin 69 (776), 114–123.

Qin, S. J., Badgwell, T. A., 2003. A survey of industrial model predictive control technology. Control Eng. Practice 11 (7), 733–764.

Ramasamy, M., Narayanan, S. S., Rao, C. D. P., 2005. Control of ball mill grinding circuit using model predictive control scheme. J. Process Control 15 (3), 273–283.

Salazar, J. L., Magne, L., Acua, G., Cubillos, F., 2009. Dynamic modelling and simulation of semi-autogenous mills. Minerals Eng. 22 (1), 70 – 77.

Soderstrom, T., Stoica, P., 1989. System Identification. Prentice Hall International, University Press, Cambridge.

Stanley, G. G., 1987. The extractive metallurgy of gold in South Africa. Vol. 1. South African Institute of Mining and Metallurgy, Johannesburg.

Wei, D., Craig, I. K., Feb. 2009. Grinding mill circuits - A survey of control and economic concerns. Int. J. Mineral Process. 90 (1-4), 56 – 66.

Whiten, W. J., 1974. A matrix theory of communition machines. Chemical Eng. Sci. 29 (2), 589–599.